*Steel and Composite Structures, Vol. 12, No. 6 (2012) 465-489*
DOI: http://dx.doi.org/10.12989/scs.2012.12.6.465


# Experimental investigation of residual stresses in cold formed steel sections

Miroslav Bešević

*Faculty of Civil Engineering Subotica, Serbia*

*(Received April 12, 2011, Revised May 03, 2011, Accepted March 24, 2012)*

**Abstract.** Residual stresses play important role for design of steel structural members. Cold formed sections usually have residual stresses caused by roll forming. When compared to stresses caused by the working load, especially for compressed members, the effects of residual stresses can be favorable or unfavorable depending on magnitude, orientation and distribution of these stresses. The research presented in this paper includes experimental investigations of residual stresses, initial imperfections and material properties on cold formed carbon steel open cross sections. Experimental results have been compared to results obtained in similar tests with stainless and high strength steel cross sections. Theoretical and experimental research, conducted for cold formed open cross sections, are important for design of axially compressed members. This paper presents two methods of residual stresses investigation: magnetic method and method of pre-drilled holes and obtained results have been compared with results of residual stresses from other authors.

**Keywords:** cold formed; residual stresses; magnetic method; pre-drilled hole method; stainless steel; high strength steel.

## 1. Introduction

### *1.1 Residual stresses*

Residual stresses have important role in calculation and design of structural steel members.

Residual stresses in structural steel are caused by uneven cooling of cross section after hot rolling and production procedures such as cold forming, pressing, welding, torch cutting, etc.

In cold formed profiles they are usually caused by the effects of cold bending during forming or pressing procedures (Besevic 1999, Weng and Pekoz 1990) and (Weng 1991, Weng and Ling 1992). Due to production differences in two types of profiles, residual stresses in cold formed profiles can be significantly different compared to the ones in hot rolled profiles.

When compared to stresses from working loads, effects of residual stresses can be harmful of beneficial depending on their magnitude, orientation and distribution.

The general influence of residual stresses on structural members is to cause premature yielding, leading to loss of stiffness and a reduction in load-carrying capacity and therefore the significance of

* Corresponding author, Professor, E-mail: miroslav.besevic@gmail.com

these effects should be considered in predicting structural behavior.

Analysis shown in this paper also includes residual stress distribution along the wall thickness of cold formed stainless profiles with box cross section that are currently widely used (Jandera *et al.* 2008) and (Jiao and Zhao 2003).

### *1.2 Initial imperfections*

One of the important factors affecting the bearing capacity of the rod is its deviation from the theoretical axis direction. Initial deviation significantly affects the load pressed composite stick, because it introduces an additional effect of bending moment, occurred under influence of normal force and the initial eccentricity $w_0$. If the initial deviation is larger than the prescribed one, then the earlier loss of bearing capacity of pressed rod may occur.

Measurements of initial curvature (straightness) of samples-profiles were performed by leveling instrument Ni 0.02 with measurements in two positions on perfectly horizontal plane. Precision of leveler was 0.2 mm on 1000 m. Measurements was performed in a laboratory on a short (3,5 m) basis. Readings were obtained by optical micrometer with precision of 1/1000 mm +/- 5/100. Compensator insured verticality of $\alpha = 0.1$". Measurement technique required a micrometer screw connected to the perfectly horizontal plate that enables 5 mm movements in a vertical plane. readings were obtained along the length of a profile so that shorter samples had 5 measurement points, middle size samples 9, longer samples 13 and longest samples had 17 measurement points both for x and y direction. Table 1 gives deflections from the profile axes. The number of samples included six samples for each slenderness.

Table 1 Measured initial imperfections for *x* and *y* directions of a *U4*

| Sample | Measurement points along the length - $v_r$ | | | | | | | | | | | | | | | $w_{0=}$ |
|---|---|---|---|---|---|---|---|---|---|---|---|---|---|---|---|---|
| | $n$ | 1 | 2 | 3 | 4 | 5 | 6 | 7 | 8 | 9 | 10 | 11 | 12 | 13 | max | $l_0/f_{max}$ |
| 4.1 | $f_y$ | 0 | -0.042 | -0.182 | -0.131 | -0.152 | -0.234 | -0.174 | 0.031 | 0.040 | 0.003 | -0.083 | 0.012 | 0 | 0.234 | 9391 |
| | $f_z$ | 0 | 0.069 | -0.049 | -0.187 | -0.387 | -0.455 | -0.486 | -0.398 | -0.236 | -0.306 | -0.374 | -0.175 | 0 | 0.486 | 4529 |
| U4.2 | $f_y$ | 0 | 0.371 | 0.692 | 1.011 | 1.194 | 1.350 | 1.139 | 0.997 | 0.956 | 0.842 | 0.540 | 0.256 | 0 | 1.350 | 1629 |
| | $f_z$ | 0 | 0.031 | -0.119 | -0.060 | 0.100 | 0.074 | 0.067 | -0.029 | -0.205 | -0.013 | 0.091 | 0.099 | 0 | 0.205 | 10744 |
| U4.3 | $f_x$ | 0 | -0.129 | -0.121 | -0.223 | -0.193 | -0.185 | -0.120 | -0.102 | -0.282 | -0.249 | -0.113 | -0.013 | 0 | 0.282 | 7807 |
| | $f_z$ | 0 | 0.099 | 0.103 | -0.131 | -0.326 | -0.060 | -0.199 | -0.285 | -0.059 | -0.217 | -0.236 | 0.124 | 0 | 0.326 | 6738 |
| U4.4 | $f_y$ | 0 | 0.039 | 0.277 | 0.293 | 0.334 | 0.340 | 0.296 | 0.260 | 0.333 | 0.432 | 0.455 | 0.314 | 0 | 0.455 | 4833 |
| | $f_z$ | 0 | 0.218 | 0.249 | 0.203 | 0.006 | -0.023 | 0.214 | 0.128 | -0.084 | -0.028 | -0.002 | -0.161 | 0 | 0.249 | 8825 |
| U4.5 | $f_y$ | 0 | 0.023 | -0.102 | -0.165 | -0.065 | -0.123 | -0.282 | -0.303 | -0.242 | -0.418 | -0.385 | -0.148 | 0 | 0.418 | 5266 |
| | $f_z$ | 0 | 0.245 | 0.078 | 0.282 | 0.049 | -0.103 | 0.082 | -0.039 | 0.008 | 0.138 | -0.173 | -0.218 | 0 | 0.282 | 7790 |
| U4.6 | $f_u$ | 0 | -0.046 | -0.072 | 0.120 | 0.144 | 0.033 | 0.154 | 0.192 | 0.241 | 0.213 | 0.032 | -0.114 | 0 | 0.241 | 9111 |
| | $f_z$ | 0 | 0.250 | 0.147 | -0.183 | -0.105 | 0.035 | 0.120 | 0.240 | 0.380 | 0.212 | 0.320 | 0.465 | 0 | 0.465 | 4729 |

Note:

| | | | |
|---|---|---|---|
| $v_r$ | Measurement points along the length | $l_0$ | sample length |
| $n$ | length section of the rod | $f_{max}$ | calculable value |
| $w_0$ | max deviation from the axis | $f_z, f_y$ | components of measured imperfections |

Structural imperfections, such as residual stresses, and geometrical imperfection, e.g., out-of-straightness, must be taken into account. For reasons of easy application all kinds of imperfection are accounted for by equivalent geometrical imperfections. These equivalent geometrical imperfections are calculated from the results of ultimate load calculations, where residual stresses, geometrical imperfections and the effect of plastification along the beam length are included (Lindner 2000). Fig. 1 shows the imperfection parameter $j$ which leads to the imperfection $w_0=L/j$ for different round-tube hollow sections as a function of the equivalent slenderness $\bar{\lambda}$. For practical applications it seems to be too complicated to use $\bar{\lambda}$ - dependent values of $j$. Therefore, for simplification has been made a table with constant values for $j$, showed in Fig. 1, these values ($j$) are calculated from the ultimate loads of centrally loaded columns.

Paper (Liu and Young 2003) investigated a box profiles made from stainless high strength steel with $\sigma_u$ = 680 MPa. Initial geometrical imperfections for box profile, series S1L and S2L, were measured for $y$ and $z$ direction and the values are shown in the Table 2.

### *1.3 Mechanical properties of steel*

Mechanical properties of steel are changed due to cold working of the virgin material. This change is material response to deformation. In order to determine the actual mechanical properties of steel ($f_y$, $f_u$, $A$, $E$) test coupons were made from base sheet and $C$ profiles. First group of samples consisted of five

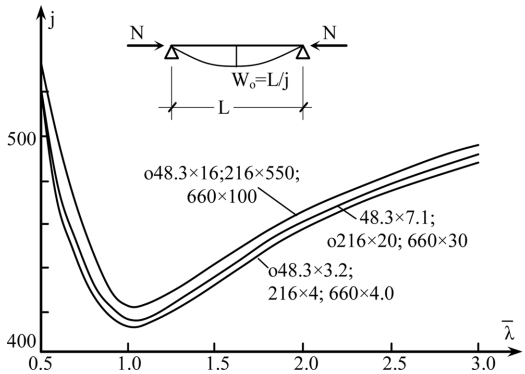


| Cross-section with European buckling curve | *j* |
|---|---|
| a | 300 |
| b | 250 |
| c | 200 |
| d | 150 |

Fig. 1 Imperfection parameter $j$ for round-tube hollow sections, using buckling curve and Table with values calculated from the ultimate loads of centrally loaded columns

Table 2 Measured overall geometric imperfections at mid-length

| Specimens | $\delta_y$ (mm) | 1/$L$ (mm) | $\delta_z$ (mm) | 1/$L$ |
|---|---|---|---|---|
| S1L1200 | 0.241 | 4970 | 0.027 | 44100 |
| S1L2000 | 0.952 | 2100 | 0.190 | 10500 |
| S1L2800 | 0.635 | 4410 | 0.063 | 44100 |
| S1L3600 | 3.789 | 950 | 0.699 | 5150 |
| S2L1200 | 0.027 | 44100 | 0.317 | 3780 |
| S2L2000 | 0.381 | 5250 | 1.904 | 1050 |
| S2L2800 | 2.545 | 1100 | 0.063 | 44080 |
| S2L3600 | 3.789 | 950 | 0.127 | 28350 |

tensile coupons obtained by cutting from the base sheet. Second group of six tensile coupons were made from the flat regions of finished profiles C90×45×20×2,5. Since most pronounced deformations in cold formed profiles are observed in corners of cross sections additional eight tensile coupons were taken from those regions ,according to the American standard AISI. All coupons were cut on the mill with constant refrigeration, in order to prevent structural changes and inducing of additional strains.

How production technology effect on mechanical characteristics of rolling steel is shown in the following summary diagrams with mean values: yield strength ($f_y$) tensile strength ($f_u$), elongation percentage ($A$) and Young's modulus ($E$), for samples extracted from the base sheet and the finished profile (Fig. 2). In corners changes are most pronounced. We can see that in comparing of yield strength values, on corners they are between 560~606 MPa, and on the straight parts of the profile ranging between 302~320 Mpa. Stress ratio of tensile to yield strength $f_u^m/f_y^m = 34\%$ on the flat part of the profile, and the corner profile $f_u^m/f_y^m = 10\%$ , where $f_u^m$ and $f_y^m$ present mean values.

According to test results for samples from the base sheet, tensile strength ($f_u$) is significantly reduced compared with test results for samples from the straight parts of finished $C$ profile.

For comparison, virgin material properties are: $f_{yl} = 277.6$ MPa, $f_u = 393.20$ MPa, A = 27%, E = 193 000 N/mm$^2$ . These are the properties from five test coupons, taken from base sheet.

Ration of tensile strength and yield limit amount to *fm*/*fe*= 34% for the straight portion of the profile while at corners it is $f_u^m / f_y^m$ =10%.

Liu and Young (2003) investigated mechanical properties for cold formed box cross sections, series

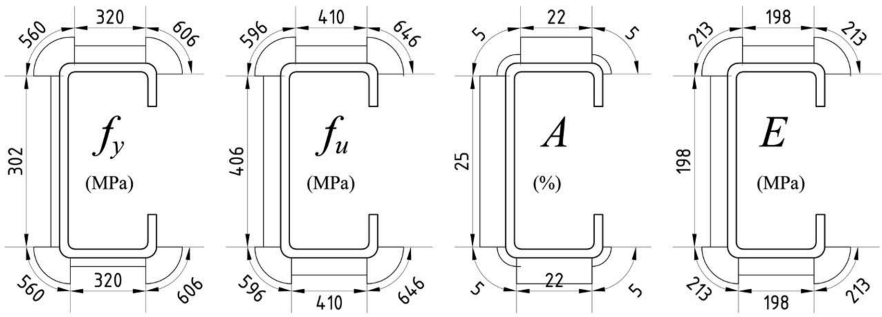


Fig. 2 Mechanical characteristics of steel

Table 3 Measured material properties from tensile coupon tests

| Series | $D\times B\times t$ (mm) | $E_0$ (GPa) | $\sigma_{0.2}$ (MPa) | $\sigma_{0.5}$ (MPa) | $\sigma_u$ MPa) | $\varepsilon_u$ (%) | $n$ |
|---|---|---|---|---|---|---|---|
| S1 | 70×70×2 | 195 | 337 | 383 | 636 | 60 | 4 |
| S2 | 70×70×5 | 194 | 444 | 500 | 688 | 61 | 5 |

Note:

| | | | |
|---|---|---|---|
| $D$ | Overall depth of square hollow section | $\sigma_{0.5}$ | Static 0.5% proof stress |
| $B$ | Overall width of square hollow section | $\varepsilon_u$ | Elongation (tensile strain) after fracture based on a gauge length of 50 mm |
| $E_0$ | Initial Young's modulus | $\sigma_u$ | Static tensile strength. |
| $\sigma_{0.2}$ | Static 0.2% proof stress | $n$ | Exponent in Ramberg–Osgood expression |

S1 70×70×2 and S2 70×70×5, with measured values of $E_0$ - modulus of elasticity and stresses. The material properties of used specimens were determined by tensile coupon tests as well as stub column tests. For tensile coupon tests, longitudinal coupons were taken from the finished specimens. The coupon dimensions conformed to the Australian Standard AS 1391 for the tensile testing of metals using 12.5 mm wide coupons of gauge length 50 mm. They obtained values of measured material properties are the static 0.2% ($\sigma_{0.2}$) and 0.5% ($\sigma_{0.5}$) proof stresses, the static tensile strength ($\sigma_u$), as well as the initial Young's modulus ($E_0$), and the elongation after fracture ($\varepsilon_u$) based on a gauge length of 50 mm. The material properties obtained from the coupon tests are summarized in Table 3.

Cold-formed stainless steel sections are formed from sheet material in two principal ways. The simplest forming process is press braking where individual folds are created in the sheet material between a tool and die. Cold rolling is a more automated process whereby sheet material is uncoiled from a roll and flattened before being fed through a series of forming rollers that gradually deform the sheet into a desired section shape. Cruise and Gardner (2008) in their research analyzed Cold-formed stainless steel sections formed in both ways and showed values as a function conventional yield limit of 0,2% × $\sigma_{0,2}$ at corners and in the flat portions (Fig. 3).

Ellobady and Young (2005) investigated measured and predicted material properties for cold formed steel sections. They used tensile coupons cut from box profiles, series SHS and RHS, from flat and corner regions (Fig. 4).

Used samples RHS1 and RHS2 were from high strength stainless steel.

Obtained values of elasticity modulus for box profiles are compatible with results conducted by Besevic (1999). Autor carried out tests on cold formed profiles C90×45×20×2.5

Values for experimentally obtained $\sigma_{0,2}$ from tensile tests obtained by different authors shows increase of strength when flat sheets are reshaped in suitable corner forms where significant plastic deformations occur during cold forming process. Increase of strength is also noticeable within flat portions of cross section, what leads to a conclusion that these portions also undergo certain plastic deformations.

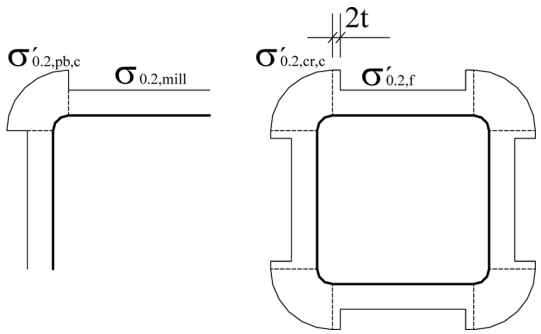


Fig. 3 Proposed 0.2% proof stress distributions for press-braked sections and cold-rolled boxes

Note:

| | |
|---|---|
| $\sigma$ '$_{0.2,f}$ | Predicted 0.2% proof stress for the central 50% of the faces of cold-rolled box sections |
| $\sigma_{0.2,mill}$ | 0.2% proof stress given in inspection document or mill certificate |
| $\sigma$ '$_{0.2.cr.c}$ | Predicted 0.2% proof stress of the corners of cold rolled box sections |
| $\sigma$ '$_{0.2.pb.c}$ | Predicted 0.2% proof stress of the corners of press braked sections |

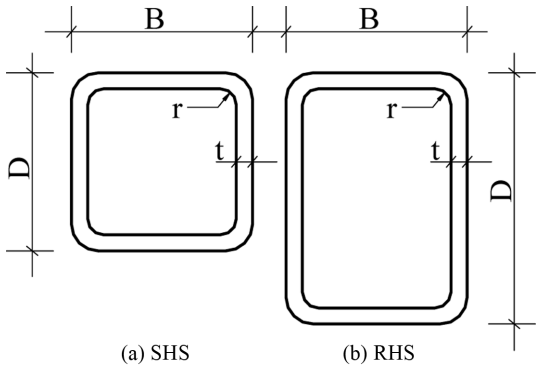


(a) SHS (b) RHS

Fig. 4 Definition of symbols for square and rectangular hollow sections

Table 4 Measured and predicted material properties (Ellobady and Young 2005)

| Test series | Section $D\times B\times t$ (mm) | Position | $\sigma_{0.2}$ (MPa) | $\sigma_u$ (MPa) | $E_0$ (GPa) | $\varepsilon_f$ (%) |
|---|---|---|---|---|---|---|
| SHS1 | 40×40×2 | Flat | 707 | 827 | 216 | 29 |
| | | Corner | 880 | 1170 | 214 | 23 |
| SHS2 | 50×50×1.5 | Flat | 622 | 770 | 200 | 37 |
| | | Corner | 744 | 1029 | 214 | 23 |
| RHS1 | 140×80×3 | Flat | 486 | 736 | 212 | 47 |
| | | Corner | 605 | 804 | 214 | 23 |
| RHS2 | 160×80×3 | Flat | 536 | 766 | 208 | 40 |
| | | Corner | 667 | 887 | 214 | 23 |

### *1.4 Residual stress analysis of structural stainless steel section*

In hot-rolled steel members residual stresses do not vary markedly through the thickness, in cold-formed members residual stresses are dominated by a 'flexural', or through thickness variation. This variation of residual stresses leads to early yielding on the faces of cold-formed steel plates. This important aspect of the load carrying behavior is completely ignored unless residual stresses are explicitly considered in the analysis.

Thin walled, cold formed steel profiles show complex behavior that is difficult to predict after reaching a buckling limit. Accuracy of numerical models is, largely, dependant on characteristic of input data that is obtained from experiments. In order to obtain additional information for the purpose of this research an existing wide range of data is collected and analyzed along with the data obtained from new experiments. According to (Schafer and Pekoz 1998) and (Narayanan and Mahendran 2003) measured values of residual stresses where membrane stresses were lower than flexural residual stresses shown in Figs. 5, 6 as function of tensile strength $f_y$. Distribution of residual stresses for two types of effects, flexural and membrane is given along the thickness of the wall for pressed and rolled cold formed profiles.

Residual stresses predominantly appear during production process and are related to differential cooling and different plastic deformations. Most significant effect of residual stresses on structural elements if appearance of early yielding which results in loss of stiffness and diminished bearing capacity. Reference (Cruise and Gardner 2008) shows an experimental program that numerically

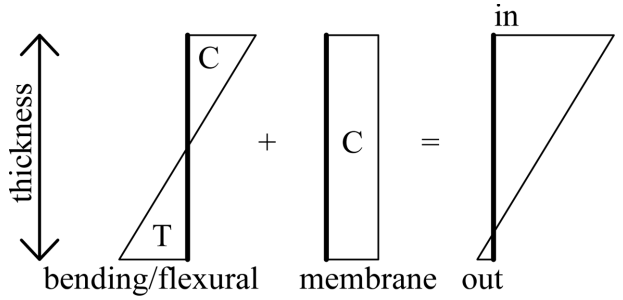


Fig. 5 Distribution of flexural and membrane residual stresses

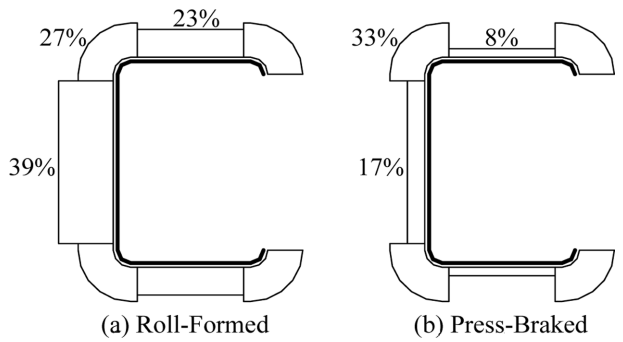


Fig. 6 Average residual stresses for pressed and press-braked profile

represents residual stresses within stainless steel cross sections produced by different production techniques. In order to determine how cold rolling effects on other types of steel comparison between stainless and carbon steel has been made. It cannot be assumed that residual stresses in stainless steel cross section are of the same magnitude as the ones in carbon steel what can be attributed to different thermal properties of stainless steel. Other differences are higher coefficient of thermal expansion, lower thermal conductivity and rounder stress-deformation curve that also has more pronounced post yield strength increase. Experiments were conducted on eight cold pressed L shape profiles and seven cold pressed box shape profiles. Measurements were conducted by electrical strain gauges while in one cross section measurements were obtained by mechanical strain gauges. Also standard tensile coupons were tested in order to determine an in-plane response of the material. Membrane residual stresses ($\sigma_m$) are mostly dominant in hot rolled and welded cross section while flexural stresses ($\sigma_b$) are dominant in cold formed cross section. Components of these two residual stresses are showed in Fig. 7, where it is assumed that flexural stress is linearly variable through the wall thickness. Combined stress ($\sigma_{rs}$) is assumed to be always linear. Most commonly, longitudinal dilatation on the inner and outer surface of the profile is measured and represented as stresses. In general, strips of material released by cutting can show axial deformations and curvatures that are related to membrane and flexural residual stresses.

The results obtained by magnetic method and by rosette strain gauges are in the range of 30 to 70% of yield strength ($f_y$), which is in accordance with results of other authors.

Compared to the carbon steel that has clearly defined yielding limit and moderate strengthening, stainless steel has curved stress-strain line with considerable strengthening and without clear yielding point. Additionally, there are in various technical properties such as: specific heat capacity, thermical conductivity, and thermical expansion. All of these have effect of residual stresses forming. Specific

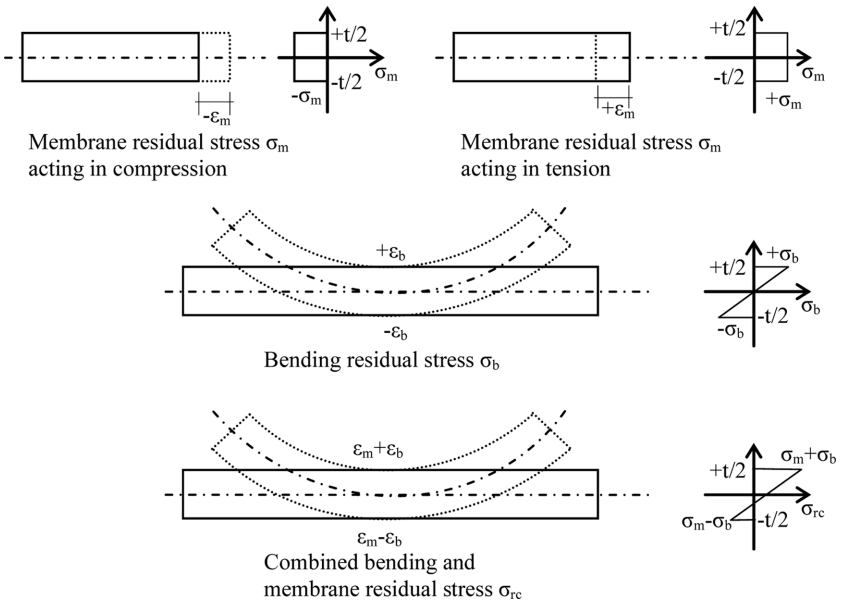


Fig. 7 Distribution of residual membrane and flexural stresses

heat capacity of stainless steel is approximately 500 J/kgK while carbon steel has this value of approx. 600 J/kgK. Material with this value lower can be heated more quickly. For temperatures below 1000 C thermal conductivity of stainless steel is lower than that of carbon steel, at lower temperatures this difference is significant while over 700 C this difference is less significant. Thermical expansion coefficient of stainless steel is up to 50% higher than that of carbon steel what can result in larger deformation of material during heating and higher residual stresses. Residual stresses for cold formed box profiles 100×50×4 mm is shown in Fig. 8

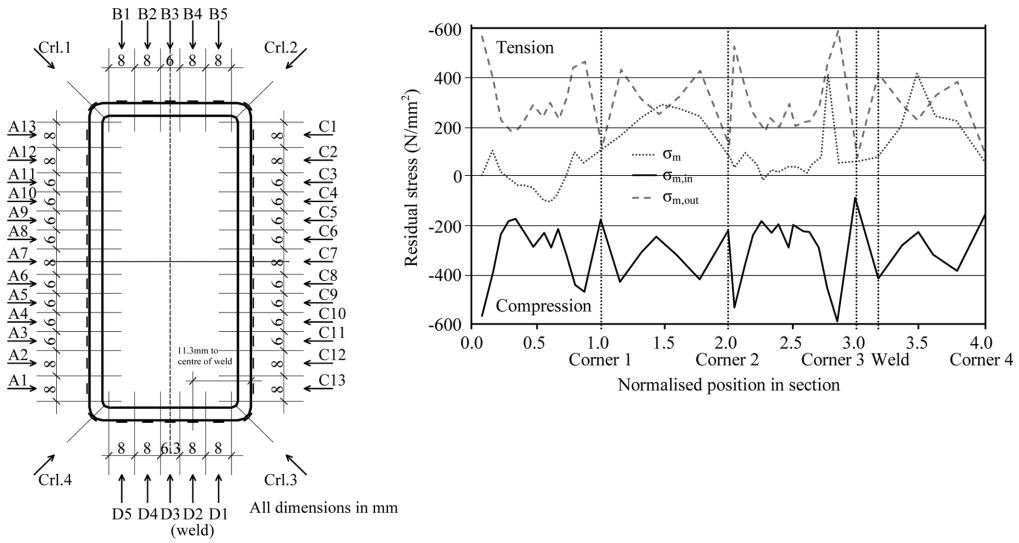


Fig. 8 Residual stresses in box shaped profile 100×50×4 mm

Residual flexural stresses $\sigma_b$ are initially determined under assumption of linear distribution along the wall thickness. Rectangular stress distribution is also taken into account. $\sigma_b = E_b \times y/R_{i\text{-}f}$, where $E_b$ is modulus of elasticity, $R_{i\text{-}f}$ is change in the curvature radius of curvature and y is the distance from the neutral axes, assumed as $t/2$, where t is material thickness for determination of stress area. Absence of symmetry in the corner fibers means that inner and outer stress areas are not equal. Residual flexural stresses have values that range from 30% to 70% of 0.2% proof stress obtained by tension tests.

Stainless steel, compared to the carbon and alloy steel has different thermic properties and behavior in compression. Considering an increase of stainless steel use in structures, it proved necessary to determine the values of residual stresses within structural members. Residual stresses have very significant presence in stainless steel cross sections.

### *1.5 Residual stresses according to EUROCODE 3*

Residual stresses have a strong effect on buckling of steel profiles what significantly reduces critical stresses. Hot rolled profiles have residual stresses due to air-cooling after hot rolling as it is shown in Table 5. Author has defined this table based on EUROCODE 1-3 and research of Victor Gioncu (2005). Profiles that were formed by welding have residual stresses due to cutting and welding processes. These are mainly membrane stresses. It is noticeable that in cold formed angle profile and pressed "C" profile values for residual stresses are very low in the flanges while in the corners can be considerable especially in the case of cold formed profiles. Residual stresses of cold formed profiles are mainly bending stresses (Table 6) and are less damaging to overall strength than membrane stresses. Stainless steel exhibits pronounced strain hardening, resulting in the corner regions of cold formed sections having 0.2% proof strengths much higher than that of the virgin material. Failure to allow for these enhanced strength regions in design leads to under-predictions of load carrying capacity. During different researches with aim to improve understanding of the structural response of stainless steel components using numerical analysis, failure to properly allow for the corner regions results in discrepancies between the predictions and the behavior observed in tests. According to ENV 1993-1-3 (1996) in the design of cold formed carbon steel sections accounts for enhanced strength corners, by allowing an increase in the average strength of the entire section. In Eqs. (1) and (2) we can see that ENV 1993-1-3 (1996) only allows strength enhancements for cross-sections that are fully effective (Ashraf *et al.* 2005)

$$f_{ya} = f_{yb} + (f_u - f_{yb}) k n t_2 / A_g \tag{1}$$

but

$$f_{ya} \leq (f_u + f_{yb})/2 \tag{2}$$

Note:

| | | | |
|---|---|---|---|
| $f_{yb}$ | nominal yield strength | $t$ | nominal core thickness |
| $A_g$ | gross cross-sectional area | $n$ | number of 90° bends in the cross-section with an internal radius $r \leq 5t$ (fractions of 90° bends should be counted as fractions of $n$) |
| $k$ | numerical coefficient that depends on the type of forming as follows:<br>$k = 7$ for cold-rolling<br>$k = 5$ for other methods of forming | | |

Table 5 Effects of forming method

| Forming method | | Hot rolling | Cold forming | |
|---|---|---|---|---|
| | | | Cold rolling | Pressing |
| Yield limit ($f_y$) | corner | no influence | considerable increase | considerable increase |
| | flange | no influence | moderate increase | no influence |
| Ultimate strength ($f_u$) | corner | no influence | considerable increase | considerable increase |
| | flange | no influence | moderate increase | no influence |

Table 6 Cold forming - membrane and bending residual stresses

| Forming method | Hot rolling | Cold forming | |
|---|---|---|---|
| | | Cold rolling | Pressing |
| Membrane residual stresses | significant | slight | slight |
| Bending residual stresses | slight | significant | slight |

## 2. Experimental analysis of residual stresses by means of magnetic method

### 2.1 Magnetic characteristics of ferromagnetic materials

According to values of relative magnetic permeability, material can be divided into three basic categories

diamagnetic $\mu_r < 1$,
paramagnetic $\mu_r > 1$ and
ferromagnetic $\mu_r >> 1$

Relative magnetic permeability is slightly different from the value 1 both in diamagnetic and in paramagnetic so, in practice, it can be adopted that $\mu_r = 1$ for such materials. Magnetic induction ($\vec{B}$) of these materials is proportional to the strength of magnetic field ($\vec{H}$). Ferromagnetic materials such as iron, nickel, cobalt, some alloys of these metals and some rare soils have their spin magnetic moment determined by their ferromagnetic properties.

Due to complex interactions within crystalline structure, spins assume parallel position what results in strong magneto-elastic effect, this means that ferromagnetic materials change their magnetic properties with the change in stress levels. Join by spot welding cause structural changes only in narrow zone around joint. This property of ferromagnetic materials is used to determine the stress state with magnetic method, assuming that structure is made from these materials. In other words, magnetic method is based on determination of changes of magnetic permeability of ferromagnetic materials caused by changes of their stress state. Relative sensitivity of magneto-elastic materials is described by the following expression

$$k = \frac{\Delta\mu/\mu}{\Delta l/l} = \frac{\varepsilon_\mu}{\varepsilon} \tag{3}$$

where:

$\mu$ - is magnetic permeability of ferromagnetic materials,
$\Delta\mu$ - change of the magnetic permeability under stresses,
$\varepsilon_\mu = \Delta\mu/\mu$ - relative magnetic permeability and
$\varepsilon$ - material strain

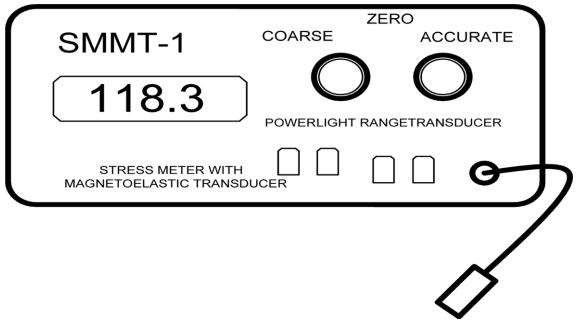


Fig. 9 SMMT-1 device for stress measurements

Although the upper expression if simple, measurements are followed by the number of difficulties such as: material inhomogenity caused, for example, by structural changes followed by welding process. Also magnetic permeability depends on the strength of the applied magnetic field(in weaker magnetic fields it increases with the stress levels while in stronger fields it decreases).

Probe consists of two solenoids that are orthogonally positioned. Solenoids have cores built from magnetic material, in order to insure higher magnetic excitation, in other words better bond with a material whose magnetic permeability is measured.

Stresses were measured with SMMT-1 device (Fig. 9). The device operates based on magneto elastic effect. Probe consists of two solenoids that are orthogonally positioned. Solenoids have cores built from magnetic material, in order to insure higher magnetic excitation, in other words better bond with a material whose magnetic permeability is measured. Probe position, which yields maximum stress, corresponds to maximum principal stress $\sigma_1$, the position and probe angle determines the angle of principal stress, $\sigma_2$ stress is obtained when probe is rotated for 90$^o$ (Milosavljevic *et al.* 1992 , Zrilic *et al.* 1998). The device measures magnetic permeability in the plain along the chosen direction due to the core orientation from one pole to another. Since magnetic permeability is proportional to the deformation which is itself proportional to stress until 0,8 $f_u$ limit ($f_u$ - yield stress), linear state measurements are possible. This direction is visibly marked on the probe. Second core measures response of 1 KHz orthogonal to that direction. This means that the device can be used to determine principal stresses and their orientation in linear state. Probe measures mean stress value over the length of ≈ 10 mm and up to a depth of 0.5 mm. This depth makes the measurements suitable for surface stresses.

Description of the measurement procedure with this device is given in the next few lines. Before measurements, the device is set to “zero”. This can be the “zero” with respect to the scale or the “zero” chosen with the calibration procedure. In the first case “zero” measurement is taken when the probe is in the air, far away from the ferromagnetic material. In the second case “zero” is set when the probe is pressed against the calibration test sample. The position and the point against which the probe is pressed are determined by the calibration position. Experience, so far, has proved that the first method is more suitable and that it is less susceptible to errors. When the “zero” is set, the measurements take place. The probe is pressed against the material surface where the stresses have to be measured. The surface of the material requires no special treatment except that it has to be flat (not necessarily smooth). The position of the probe at which the maximal stress is measured corresponds to maximal main stress $\sigma_1$, based on the position of the probe an angle of this stress is determined while the stress $\sigma_2$ is obtained when the probe is rotated by 90$^o$.

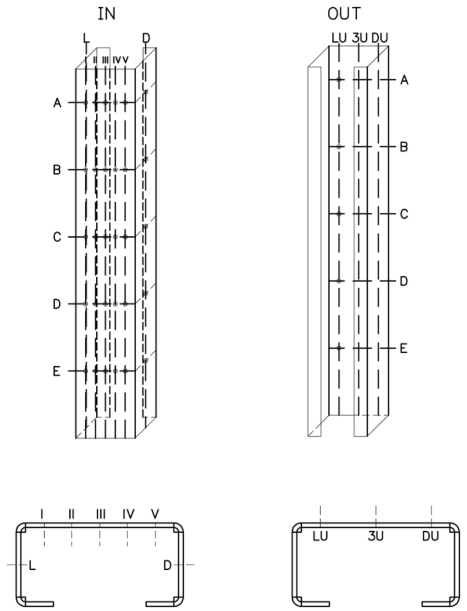


Fig. 10 Layout of inner and outer measuring points

Table 7 Principal normal stresses measured on the outer surface of the profile (given in a crosswise direction)

| Measure-ment point | Point distance | L | V | IV | III | II | I | D | SR |
|---|---|---|---|---|---|---|---|---|---|
| | | $\sigma_1$ | $\sigma_1$ | $\sigma_1$ | $\sigma_1$ | $\sigma_1$ | $\sigma_1$ | $\sigma_1$ | $\sigma_1$ |
| | mm | MPa | MPa | MPa | MPa | MPa | MPa | MPa | MPa |
| A | 15 | 78 | 267 | 130 | 112 | 164 | 198 | 164 | 159 |
| B | 115 | 52 | 198 | 164 | 147 | 112 | 233 | 95 | 143 |
| C | 215 | 112 | 130 | 61 | 104 | 61 | 112 | 147 | 104 |
| D | 385 | 26 | 190 | 112 | 61 | 52 | 181 | 198 | 117 |
| E | 485 | 95 | 259 | 95 | 147 | 164 | 181 | 181 | 160 |
| | | 72.6 | 208.8 | 112.4 | 114.2 | 110.6 | 181 | 157 | 136.6 |

Table 8 Principal normal stresses measured on the outer surface of the profile (given in a lengthwise direction)

| Measurement point | Point distance | A | B | C | D | E | SR |
|---|---|---|---|---|---|---|---|
| | | $\sigma_1$ | $\sigma_1$ | $\sigma_1$ | $\sigma_1$ | $\sigma_1$ | $\sigma_1$ |
| | mm | MPa | MPa | MPa | MPa | MPa | MPa |
| L | 22.5 | 78 | 52 | 112 | 26 | 95 | 73 |
| 5 | 60 | 267 | 198 | 130 | 190 | 259 | 209 |
| 4 | 75 | 130 | 164 | 61 | 112 | 95 | 112 |
| 3 | 90 | 112 | 147 | 104 | 61 | 147 | 114 |
| 2 | 105 | 164 | 112 | 61 | 52 | 164 | 111 |
| 1 | 120 | 198 | 233 | 112 | 181 | 181 | 181 |
| D | 157.5 | 164 | 95 | 147 | 198 | 181 | 157 |
| | | 159 | 143 | 103.8 | 117.1 | 106.3 | 136.7 |

Table 9 Principal normal stresses measured on the inner surface of the profile (given in a lengthwise direction)

| Measurement point | Point distance | A | B | C | D | E |
|---|---|---|---|---|---|---|
| | | $\sigma_1$ | $\sigma_1$ | $\sigma_1$ | $\sigma_1$ | $\sigma_1$ |
| | mm | MPa | MPa | MPa | MPa | MPa |
| LU | 22.5 | -171 | -180 | -163 | -189 | -180 |
| 3U | 90.0 | -128 | -137 | -120 | -111 | -111 |
| DU | 127.5 | -163 | -171 | -154 | -180 | -180 |

Measurements by means of magnetic method within the scope of this research were performed in the Laboratory of Faculty for Metallurgic Technology in Belgrade on specially made samples. Measurement points are defined in five cross sections lengthwise with seven points crosswise. Outer and inner measurements points are shown in the Fig. 10. Obtained values are mmeasured in the flat parts of profile on a sufficiently large distance in order to prevent influences of surrounding sides of the section.

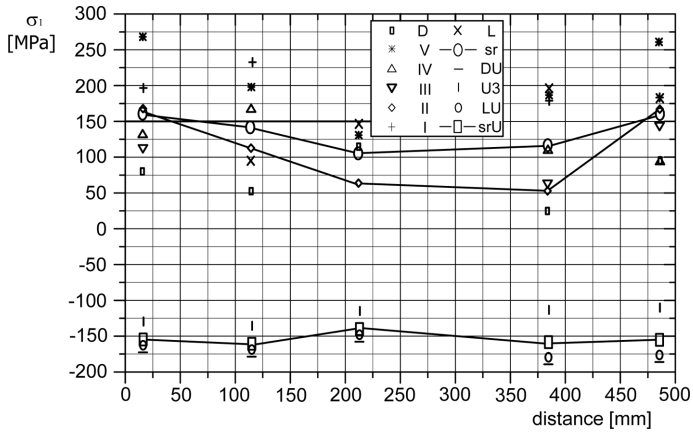


Fig. 11 Residual stresses shown with respect to length of the profile ($\sigma_r$ - mean value of residual stresses)

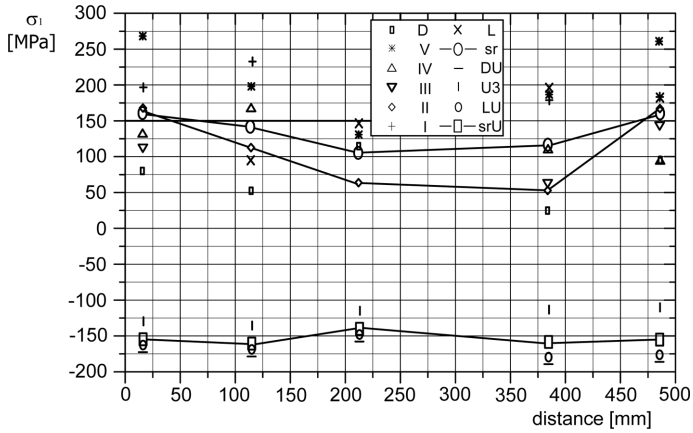


Fig. 12 Residual stresses, measured on the outer and on the inner surface of the profile. Shown with respect to lengthwise direction of the profile ($\sigma_r$ - mean value of residual stresses)

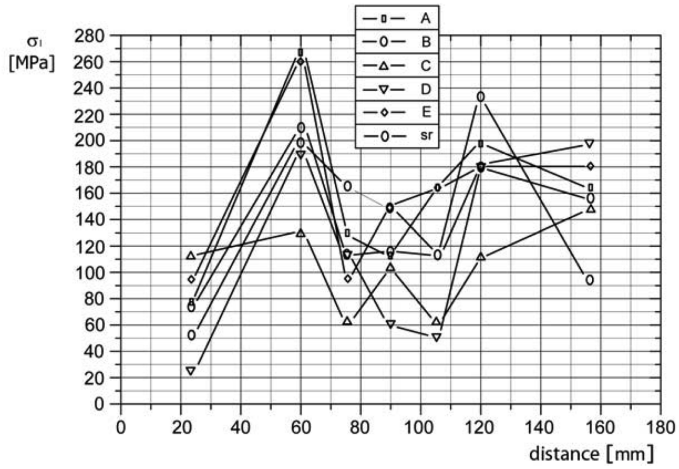


Fig. 13 Residual stresses shown with respect to lengthwise direction of the profile ($\sigma_r$ - mean value of residual stresses)

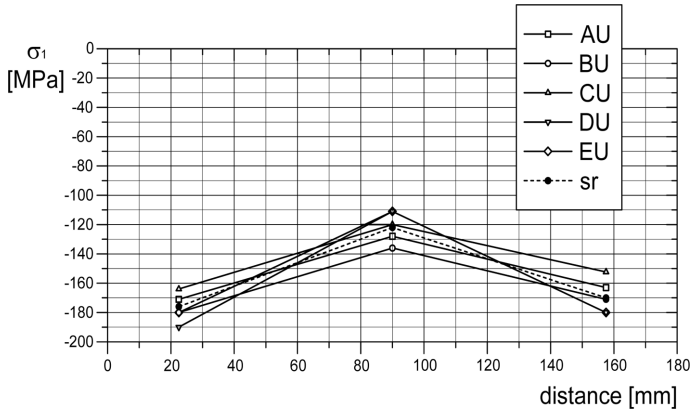


Fig. 14 Inner residual stresses shown with respect to crosswise direction of the profile ($\sigma_r$ - mean value of residual stresses)

Measured and calibrated values of residual stresses are given in Tables 7, 8 and 9. Figs. 11, 12, 13 and 14 show outer and inner residual stresses.

Based on obtained test results could be conclude that the value of surface tension of sections range between approximately 25 and 70% of yield stress materials. Values for inner stress on the flat parts of the section are approximately evenly distributed on the section volume. We could also see that those values are in angles higher than those on the flat parts and that difference is approximately 15~30% of yield stress materials. It was found that the magnitude in the same place of inner stress on the inside and outside of the flat parts of approximately equal. The general pattern of the distribution of inner stress follows a consistent model for all samples. The values of surface stress in the cross-transversal direction were almost 2 times higher than those in the longitudinal direction.

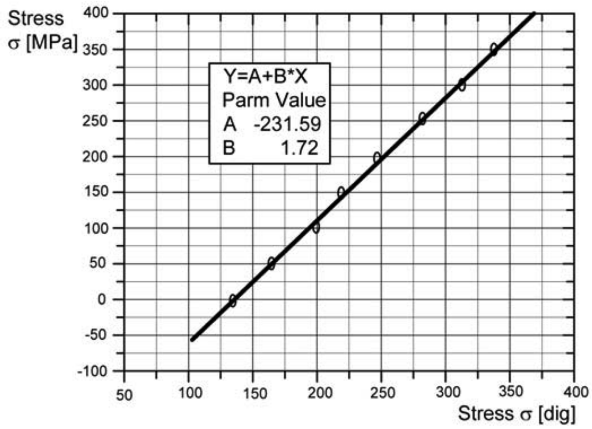


Fig. 15 Calibration cure for Altern 55 material

### 2.2 Calibration

Determination of calibration curve requires a standard test sample for tension tests, with rectangular cross section and a minimal width of 25 mm. It must be made from the same material as the one from the structure. This material has to be undisturbed. Test sample is subjected to a tension test up to 0,8 $f_y$. Testing is performed through gradual increase of load followed by simultaneous recording of load value and appropriate magnetic characteristic value, expressed in numbers or dig. Calibration equation can be written as follows

$$Y(MPa) = -231.59 + 1.72 \times (dig) \tag{4}$$

## 3. Measurement of residual stresses with rosette strain gauges

The pre-drilled hole method is a technique that is in widest use for measurement of residual stresses. This method requires, after the deformation sensors have been installed on the surface of the specimen, a shallow little hole to be drilled on the surface of the specimen. After drilling, the change of strain in the vicinity of the hole is measured which is the basis for the calculation of released residual stress. This method belongs to semi destructive category, because a little hole usually cannot deteriorate integrity of the structure. Holes are usually 1.5~3.0 mm in diameter and of the same depth.

After drilling the hole measurements should be taken on all three strain gauges in the rosette. These values are later used for determination of the principal normal stresses $\sigma_1$ and the anglej. Beside measured values, it is necessary to determine $A$ and $B$ constants, which take into account the geometric layout of the gauges and the diameter of the hole. Calculation is based on the following expressions (Milosavljevic *et al.* 1992)

$$A = \frac{a^2 \cdot (1+v)}{2r_a \cdot r_i} \tag{5}$$

$$B = \frac{2a^2}{r_a \cdot r_i} \cdot \left[1 - \frac{a^2(1+\nu) \cdot (r_a^2 + r_a r_i + r_i^2)}{4r_a^2 \cdot r_i^2}\right] \tag{6}$$

where symbols are defined as follows:

$\nu$ - Poisson coefficient,

$r_a$ - net outer radius of the strain gauge,

$r_i$ - net inner radius of the strain gauge,

$a$ - radius of drilled hole.

For this investigation, 6/120 RY 61 strain gauge (rosette) was used. It has an outer radius of $r_a = 3.3$ mm and the inner one of $r_i = 1.8$ mm. Therefore, equations for $A$ and $B$ can be written as follows (Milosavljevic *et al.* 1992)

$$A = \frac{a^2(1+\nu)}{11.88} \tag{7}$$

$$B = \frac{a^2}{2.97} \cdot [1 - 0.1422a^2(1+\nu)] \tag{8}$$

The hole diameter is in this case 0.75 mm so constants $A$ and $B$ are

$$A = 0.04735 \cdot (1+\nu) \tag{9}$$

$$B = 0.1894 - 0.01515 \cdot (1+\nu) \tag{10}$$

These values for constants $A$ and $B$ are then transformed into new form $A^*$ and $B^*$ where:

$$A^* = \frac{E}{4A} = \frac{E}{0.1894 \cdot (1+\nu)} \tag{11}$$

$$B^* = \frac{E}{4B} = \frac{E}{0.7576 - 0.0606 \cdot (1+\nu)} \tag{12}$$

The stresses are calculated with following equation

$$\sigma_{1,2} = -A^*(\Delta\varepsilon_a + \Delta\varepsilon_c) \pm B^* \sqrt{(\Delta\varepsilon_a + \Delta\varepsilon_c - 2 \cdot \Delta\varepsilon_b)^2 + (\Delta\varepsilon_c - \Delta\varepsilon_a)^2} \tag{13}$$

The values $A^*$ and $B^*$ can be found in the Table 10 for various values of Young's modulus of elasticity $E$ and Poisson's rations $\nu$. These values pertain to the geometric parameters of the rosette RY 61 and the hole diameter 2a = 1.5 mm.

Table 10 Values of Young's modulus for the steel (Milosavljevic *et al.* 1992)

| | $A^*$ | | | $B^*$ | | |
|---|---|---|---|---|---|---|
| E (MPa) | ν=0.26 | ν=0.30 | ν=0.34 | ν=0.26 | ν=0.30 | ν=0.34 |
| 210000 | 879972 | 852896 | 827436 | 308259 | 309360 | 310049 |

The angle φ is calculated as follows

$$tg2\varphi = \frac{\Delta\varepsilon_a + \Delta\varepsilon_c - 2 \cdot \Delta\varepsilon_b}{\Delta\varepsilon_c - \Delta\varepsilon_a} \tag{14}$$

$$\varphi = \frac{1}{2} arctg \frac{\Delta\varepsilon_a + \Delta\varepsilon_c - 2 \cdot \Delta\varepsilon_b}{\Delta\varepsilon_c - \Delta\varepsilon_a} \tag{15}$$

All these values give us the basis to calculate the principal normal stresses $\sigma_1$ and $\sigma_2$.
The rosette RY61 was mounted so that the gauge "a" (Fig. 16) is pointed to the axes of reference.

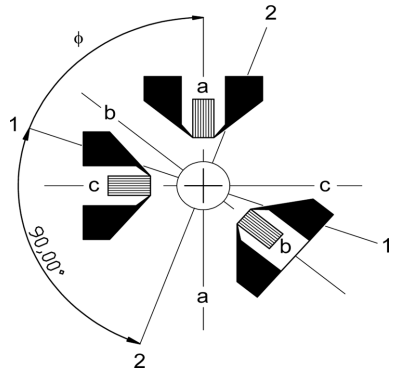


Fig. 16 Strain gauge - rosette RY61

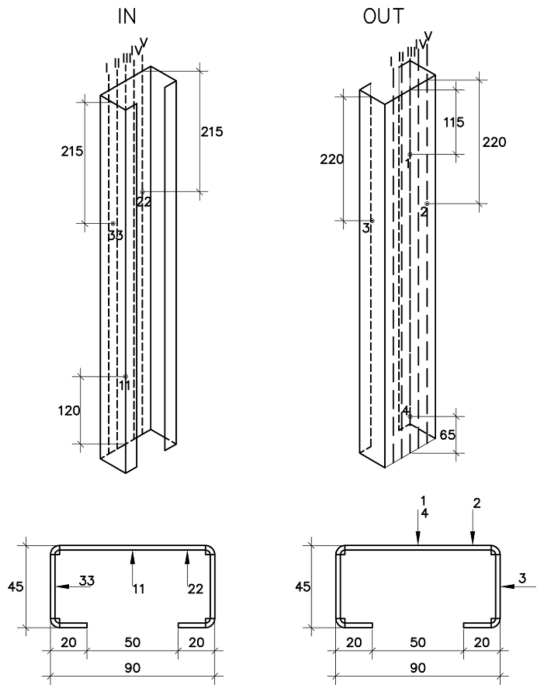


Fig. 17 Disposition of Strain gauge - rosette RY61 on sample

Table 11 Measured residual stresses (own measurements)

| Measurement point | Gauge 1 | Gauge 2 | Gauge 3 | Stress $\sigma_1$ (MPa) | Stress $\sigma_2$ (MPa) | Angle φ |
|---|---|---|---|---|---|---|
| 1 | -74 | -86 | -12 | 106.1 | 40.6 | 27.1 |
| 2 | -48 | -174 | -16 | 143.0 | -33.8 | 41.8 |
| 3 | -49 | -120 | -19 | 112.0 | 4.0 | 40.1 |
| 4 | -58 | -100 | -25 | 108.4 | 33.2 | 37.1 |
| 11 | 155 | 55 | 45 | -126.6 | 136.3 | -19.7 |
| 22 | 283 | 148 | 83 | -246.6 | 231.1 | -9.6 |
| 33 | 214 | 124 | 70 | -196.3 | 180.5 | -7.0 |

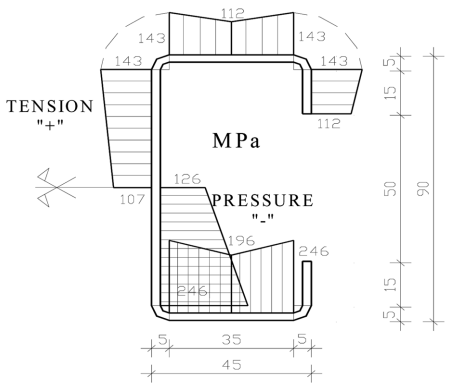


Fig. 18 Residual stresses measured on the inner and outer surface of the profile

Fig. 19 Application of the rosette strain gauge - measuring point 1

## 4. EDM testing method

Electric discharge machining (*EDM*) is also known as electric corrosion procedure. Because it is based on the principle of erosion of metal as a result of electric discharge. In *EDM* procedure, a material is being removed by a series of discrete electric discharges that appear in the space between electrode (blade) and the object (specimen). When fluid between two closest points is ionized, dielectric fluid

forms a discharge route. Discharge starts when additional amount of electric charge is introduced to the interspace, which causes ionization of dielectric fluid and electric current. Dielectric fluid also serves as a coolant and for the transport of residual waste of the testing procedure. Because of this, there is no mechanical effect on the specimen unlike in the saw-cutting procedure; this also minimizes the overheating problem due to cutting. *EDM* technique for residual stress measurements does not require so tight fixing in the clamp during cutting. This makes it possible to overcome the problem of too tight fix of the thin walled profiles. Weg and Pekoz had an experimental investigation of the residual stresses in cold formed steel members with *EDM* technique. Their results, presented in Table 13, provide a further understanding of the magnitude and distribution of the residual stresses in cold formed sections. Test coupons have properties like CR220 class of steel with properties: $f_y$ = 220 MPa, $f_u$ = 300 MPa , or as EN10268(H240LA) with values $f_y$ = 240 MPa, $f_u$ = 340 MPa.

Fig. 20 shows the results of measured surface residual stresses in the longitudinal direction of the specimen. Measured negative deformation corresponds to residual tension stress within the specimen while positive deformation corresponds to residual compression stress (Weng 1991, Weng and Ling 1992)

## 5. Comparasion of results obtained by magnetic method, strain gauges and EDM method

Graphical representation of the residual stresses obtained by magnetic method (*MM*) and by strain gauges (MT) is compared to Weng Pekoz results and given in Figs. 21 and 22.

Samples used in testing by magnetic method (*MM*) and strain gages method(*MT*) are in IV class of steel hardness with: $f_{ym}$ = 300 MPa , $f_{um}$ = 406 MPa in flat part of finished profile *C*, and obtained results are similar to results obtained by Weng Pekoz.

Table 12 Cross section properties of tested members

| | $t$ [mm] | $A$ [mm$^2$] | $a$ [mm] | $b$ [mm] | $c$ [mm] | $r$ [mm] | $\sigma_y$ [MPa] | $\sigma_u$ [MPa] |
|---|---|---|---|---|---|---|---|---|
| P11 | 3.07 | 33.73 | 127.94 | 63.27 | 22.30 | 3.175 | 231.00 | 357.66 |
| (P16) | 1.62 | 10.03 | 67.18 | 34.97 | 15.82 | 2.387 | 220.89 | 310.67 |

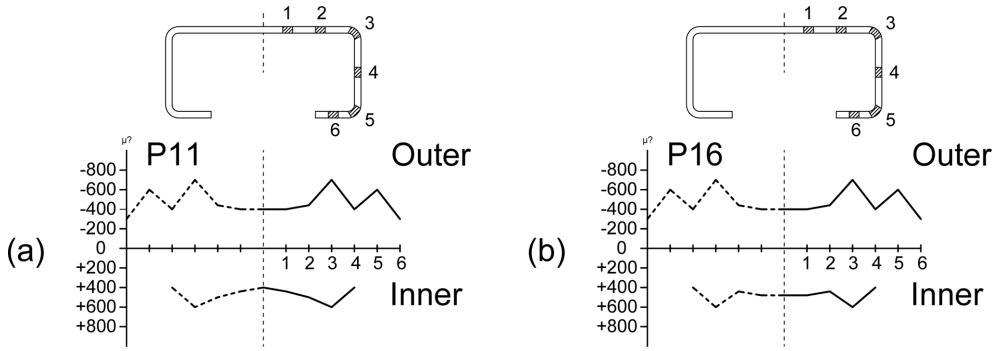


Fig. 20 Measured residual stress (a) cross section P11 and (b) cross section P16

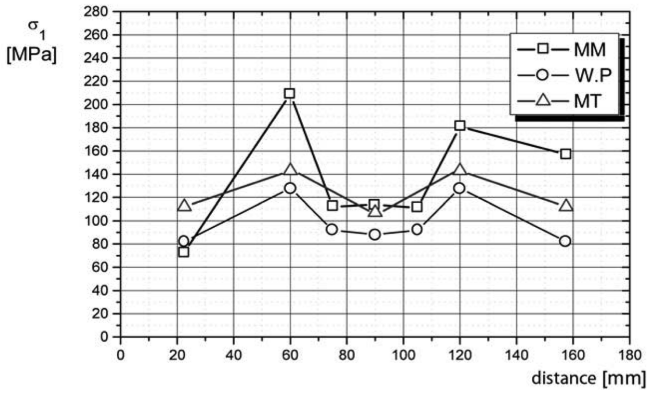


Fig. 21 Residual stresses measured on the outer surface of the profile (outer)

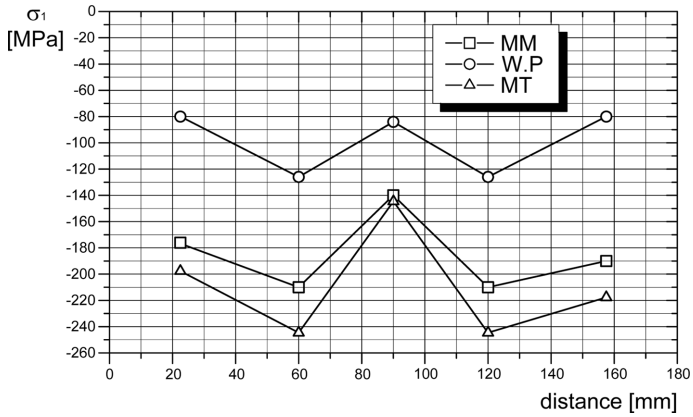


Fig. 22 Residual stresses measured on the outer surface of the profile (inner)

## 6. Measurement of residual stresses by x-ray diffraction

Paper (Jandera *et al.* 2008) shows the distribution of residual stresses along the wall thickness of cold formed stainless steel cross section that is determined by the x-ray diffraction and the effect of residual stresses was estimated through detailed nonlinear numerical modeling. In recent years an increase in demand of high-alloyed steel, including high strength steel and stainless steel, for use in structural engineering. Presented research investigates cold-formed cross sections from stainless steel that are widely used as compressed structural members. Stainless steel shows different properties compared to carbon steel such as: nonalloy and nonsymmetrical stress-strain behavior, anisotropy, pronounced response to cold forming process, different effect of initial imperfection and different thermical properties, therefore different distribution of residual stresses and their effect on structure. Residual stresses of highest magnitude were observed in cold formed box cross sections.

X-ray method is based on measurement of changes of distance between the planes of crystal trusses within the microstructure of the material, thus revealing elastic deformations, surface stress can be determined up to a depth of 5~10 microns. For measurement along the depth, individual layers must be

removed by means of electrolytes. For these measurement and X-ray of 1.8 mm diameter was used, together with 10 mm sample of oscillation along the longitudinal axes of the sample in order to improve measurement reliability. In total, 20 surface measurements and two measurements up to a one-half of wall thickness of profile 100×80×2. Successful measurements were performed in directions parallel and orthogonal to the rolling direction. Surface measurements showed a thin layer of compressive residual stresses on the outer profile surface, which are assumed, appear due to the contact with the shaping tool and can be beneficial regarding the resistance to corrosive stresses-cracking. Values of orthogonal surface stresses are two times higher than those in longitudinal direction. Two measurements along the thickness of the wall were performed in the point 3 (welding spot) and point 1 (8 mm from the weld). In general, tensile stresses are represented on the outer surface of the sample wall with isolation of the, above mentioned, thin compressed layer. These stresses, seem to have a uniform distribution along the one half of the thickness and therefore can be represented by the rectangular block distribution, proposed after determine residual stresses magnitudes from the surface strain released by cutting.

Figs. 23 and 24 show initial stress distribution that was used for modeling.

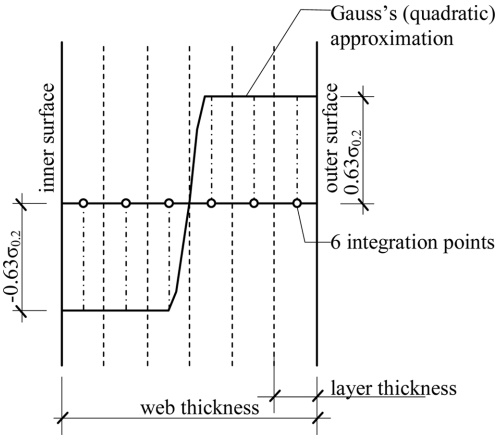


Fig. 23 Initial residual stress distribution along the wall thickness for FE modeling

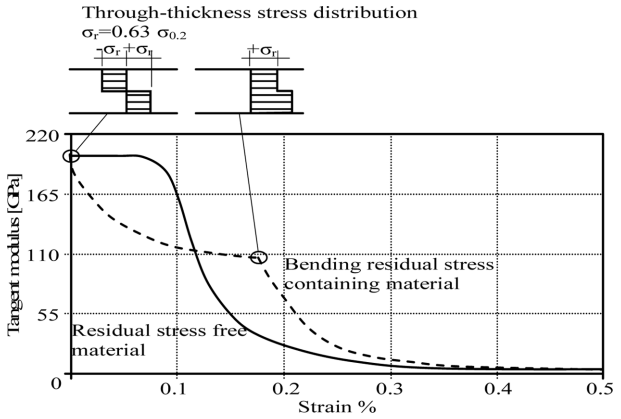


Fig. 24 Stress distribution along the wall thickness with and without residual stresses

## 7. Stub-column test

Gardner and Nethercote (2004) investigated stub-column test, with square and rectangular cross sections of stainless steel samples, in order to compare yield strength and yield stress of the finished profiles.

Apart from residual stresses, initial imperfection and mechanical properties significant parameter is compression yield limit that can be obtained from stub-column tests. Steel columns that were the subject of this research consist of two profiles that form complex cross section, Fig. 25. Profiles that make cross section of columns in question were produced by means of cold forming. This production process demands in depth investigation such as this one, especially because cold forming induces changes in material mechanical properties and residual stresses in the cross section. Yield limits, tensile stress limits, elasticity modulus and elongation percentage acquired by standard tensile coupon tests cannot represent the whole cross section, in other word its average stress-strain curve. In this case, average yield limits were determined through compression tests of stub columns. Stub columns samples investigated in this research were designed so that they are short enough not to include slenderness effects but long enough to include preserve initial magnitude and distribution of the residual stresses. Investigation into behavior of the stub columns reveals also a local buckling effects, as well as effects of cold forming on the bearing capacity of the column. Height of the stub columns was 366.3 mm in other words 15 λ. Tests were conducted on digitally guided press Amsler 5000 KN at the Institute for material testing of Serbia. Centricity of the applied force was enabled by spherical bearings and centrically monitored geometrical position.

Two samples were tested with 12 strain gauges each while measurements on other four samples included only maximum force and deformation in two directions orthogonal to the columns axes by means of electronic dial gauges. Measurements of the force-strain and force-deformation diagrams was conducted by means of computer software, in other word force was electronically monitored. Fig. 25. shows stub column testing with measurement equipment.

Tests revealed a modulus of elasticity and values of maximal force. Two samples were subjected to cyclic loads and diagrams force-deformation and force-strain during those tests are shown in Fig. 26. Table 13. gives the analysis of deviation between experimentally obtained data for axial bearing capacity of stub columns based on the global yielding and yield limits obtained by standard coupon tests of the input basic steel plate before cold forming (coupons $f_y$).

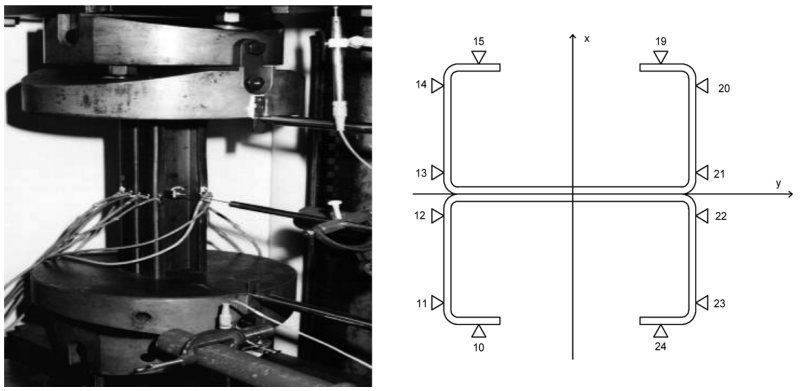


Fig. 25 Stub column during test and its cross section with position of strain gauges

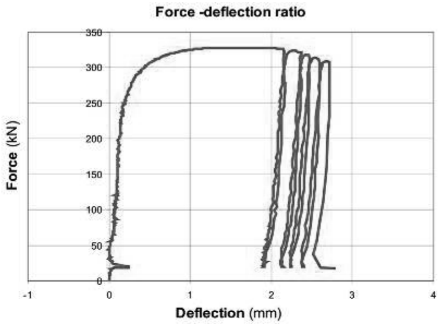


Fig. 26 Diagram force-deformation and force-strain under cyclic loads

Table 13 Differences between experimentally obtained values from standard tensile coupons from basic material $f_{yl}$ and stub column tests based on global yielding $\sigma_t$

| Stress in basic tensile coupon and in the stub column | U11 | U12 | U13 | U14 | U15 | U16 | Average value |
|---|---|---|---|---|---|---|---|
| Basic coupon $f_{yl}$ (MPa) | 272.0 | 264.0 | 299.0 | 281.0 | 272.0 | - | 277.6 |
| Stub column $\sigma_t$ (MPa) | 321.4 | 323.0 | 324.7 | 330.0 | 326.2 | 32.90 | 325.7 |
| Difference $\sigma_t$ (MPa) | 49.4 | 59.0 | 25.7 | 49.0 | 54.2 | - | 48.1 |
| Difference (%) | 153.6 | 182.7 | 79.2 | 148.6 | 166.1 | - | 14.77 |

$\sigma_t$ : yield point

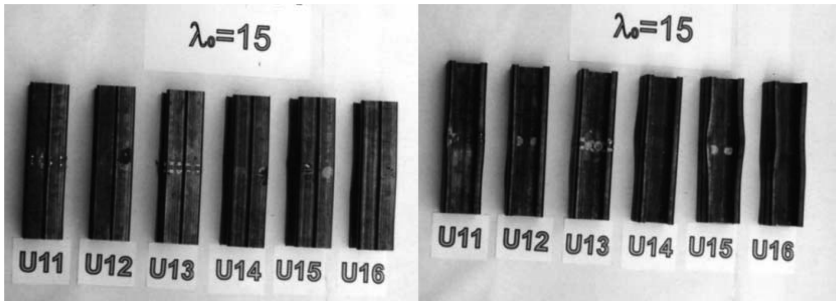


Fig. 27 Stub column samples after testing

## 8. Conclusions

Analysis and results of own experimental research into residual stresses of cold formed profile C90×45×20×2,5 used for forming a complex cross section profiles that were used in research of compressed members, yielded necessary input data for calculation of bearing capacity of axially compressed members. Research results include two methods that can be combined in order to determine residual stresses. Magnetic method is simple and cost effective, it is less accurate and it is used within fixed boundaries of ±40 MPa. More accurate method for residual stress measurement is the rosette strain gauge and pre-drilled hole method. Rational choice of measuring points with considerations of symmetry it is possible to obtain precise measurements on the sample. It is possible to

reduce the measurement costs by combining magnetic and rosette strain gauge method. First, it is necessary to perform magnetic method measurements on as many samples as possible, and then perform a check of residual stresses on some measurement points with rosette strain gauge method.

Own research of residual stresses on "*C*"- profile are compared with research performed by Weng and Pekoz on similar "*C*" - profiles with electric discharge method (*EDM*). Mechanical properties of steel were different but obtained residual stresses have a matching shape (Figs. 21, 22). This match is most obvious on the wing of "*C*" profile. Residual stresses that were obtained with this research enable us to design stability of axially compressed member with greater accuracy. As it was noted in the paper the impact of higher residual stresses in the corners can be reduced with increased yield limit. Beside that corner area is a minor part of the whole surface of cold formed cross-section, so it is reasonable to use uniform value of residual stresses along the length of the profile for calculation.

Residual stresses on the outer edge of the profile are tension stresses while inner residual stresses are in compression.

Based on the latest research according to Schafer and Pekoz (1998), Jandera *et al.* (2008), Cruise *et al.* (2008), Cruise and Gardner (2008) and use of FEM it is shown that residual stresses along the depth of the wall follow have a rectangular block shape.

Initial geometrical imperfections were measured for "*C*" cross sections, box cross sections of square and rectangular shape and circular cold formed cross sections. Significant number of tests was conducted in order to obtain changes of mechanical properties of steel because of production technology - by rolling or pressing and average values. Material properties of flat and corner portions of the cross sections were analyzed and compared with existing research.

Paper describes experimental and numerical analysis of structural members from stainless steel with special consideration of residual stresses. X-ray diffraction was used for determination of shape of distribution of residual stresses in hollow cross sections. Thin surface layer of residual stresses was detected that spreads along the whole outer surface of the profile and it is assumed that it is caused by application of high forces during rolling process. At the rest of the outer half of the wall, thickness tensile stresses were detected and measurements confirm rectangular block shape residual stress distribution(Jandera *et al.* 2008).

X-ray method is based on measurement of changes of distance between the planes of crystal trusses within the microstructure of the material, thus revealing elastic deformations, surface stress can be determined up to a depth of 5~10 microns. For measurement along the depth, individual layers must be removed by means of electrolytes. For these measurement and X-ray of 1.8 mm diameter was used, together with 10 mm sample of oscillation along the longitudinal axes of the sample in order to improve measurement reliability. Surface measurements showed a thin layer of compressive residual stresses on the outer profile surface, which are assumed, appear due to the contact with the shaping tool and can be beneficial regarding the resistance to corrosive stresses-cracking. Values of orthogonal surface stresses are two times higher than those in longitudinal direction. These stresses, seem to have a uniform distribution along the one half of the thickness and therefore can be represented by the rectangular block distribution.

Obtained results of stub cold formed column tests represent necessary input data for numerical analysis of centrically compressed members that includes geometrical and material nonlinearity. Shape of the force-strain diagram obtained by the stub column tests can be similar to correspondent diagram obtained by tensile tests only in the case of stub columns of full cross section at which the effect of strengthening is manifested by the lack of local buckling. This research showed a global yield limit of complex cross-section which is compared to the yield limit $fy_1$ obtained from tensile coupon tests. In addition, a real

modulus of elasticity for the material was obtained. Average percentage of increase of yield limit in relation to high strain limit for tested samples of the series 1 was determined to be 14.77%.

## References

Ashraf, M., Gardner, L. and Nethercot, D.A. (2005), "Strength enhancement of the corner regions of stainless steel cross- sections," *J. Constr. Steel. Res.*, **61**(1), 37-52.

Besevic, M. (1999), "Contribution to analysis of axially compressed cold formed steel members," doctoral thesis, Belgrade, Serbia.

Cruise, R.B. and Gardner, L. (2008), "Residual stress analysis of structural stainless steel section," *J. Constr. Steel. Res.*, **64**(3), 352-366.

Cruise, R.B. and Gardner, L. (2008), "Strength enhancements induced during cold-forming of stainless steel sections," *J. Constr. Steel. Res.*, **64**(11), 1310-1316.

Ellobady, E. and Young, B. (2005), "Structural performance of cold-formed high strength stainless steel columns," *J. Constr. Steel. Res.*, **61**(12), 1631-1649.

EN 1993-1-3. (2006), Eurocode 3: Design of Steel Structures-Part 1.3: General rules. Supplementary rules for cold formed thin gauge members and sheeting. European Standard,CEN.

EN 1993-1-4. (1996), Eurocode 3: Design of Steel Structures-Part 1.4: General rules. Supplementary rules for Stainless steels. European Standard,CEN.

Gardner, L. and Nethercot, D.A. (2004), "Experiments on stainless steel hollow sections-Part 1: Material and cross-sectional behavior," *J. Constr. Steel. Res.*, **60**(9), 1291-1318.

Gioncu, V. and Pignataro, M. (2005), "Phenomenological and Mathematical Modelling of Structural Instabilities," Springer, ISBN-10:3211252924, ISBN-13:978-3211252925.

Jandera, M., Gardner, L. and Machacek, J. (2008), "Residual stresses in cold-rolled stainless steel hollow sections," *J. Constr. Steel. Res.*, **64**(11), 1255-1263, doi:10.1016/j.jcsr.2008.07.022.

Jiao, H. and Zhao, X.-L. (2003), "Imperfection, residual stress and yield slenderness limit of very high strength (VHS) circular steel tubes," *J. Constr. Steel. Res.*, **59**(2), 223-249.

Lidnder, J. (2000), "Stability of structure members-General report," *J. Constr. Steel. Res.*, **55**(11-3), 29-44.

Liu, Y. and Young, B. (2003), "Buckling of stainless steel square hallow section compression members," *J. Constr. Steel. Res.*, **59**(2), 165-177.

Milosavljevic, A., Prokic, R., Smiljanic, P., Zrilic, M. and Kerecki, P. (1992), "Evaluation of residual stresses in welded steel constructions," ECF9, Reliability and structural integrity of advanced materials, EMAS, Warley, West Midlands, Vol. II, U.K,

Narayanan, S. and Mahendran, M. (2003), "Ultimate capacity of innovative cold –formed steel columns," *J. Constr. Steel. Res.*, **59**(4), 489-508.

Schafer, B.W. and Pekoz, T. (1998), "Computation modeling of cold–formed steel: characterizing geometric imperfection and residual stresses," *J. Constr. Steel. Res.*, **47**(3), 193-210.

Weng, C.C. (1991), "Effect of residual stress on cold-formed steel column strength," *J. Struct. Eng.*, **117**(6), June, ASCE, ISSN 0733-9445/91/0006-1622/Paper No. 25877.

Weng, C.C. and Ling, C.P. (1992), "Study on maximum strength of cold-formed steel columns," *J. Struct. Eng.*, **118**(1), January, ASCE, ISSN 0733-0445/92/0001-0128/Paper No. 340.1611/Paper No. 24766.

Weng, C.C. and Pekoz, T. (1990), "Residual stresses in cold formed steel members," *J. Struct. Eng.*, **116**(6), June, ASCE, ISSN 0733-9445/90/0006-

Zrilic, M., Rakin, M., Milovic-Matic, L.J. and Putic, S. (1998), "Determination of Residual Stresses in the Welding Area of the Cylindrical Rotary Furnice Cover," International Symposium on Pipeline Welding, Pipeline Welding '98, Istanbul, Turkey,